Research Article

Abdur Rauf*, Zubair Ahmad, Haiyuan Zhang*, Naveed Muhammad, Zuneera Akram, and Inam Ud Din

Green synthesis, characterization, and *in vitro* and *in vivo* biological screening of iron oxide nanoparticles (Fe_3O_4) generated with hydroalcoholic extract of aerial parts of *Euphorbia milii*

https://doi.org/10.1515/gps-2024-0155
received August 09, 2024; accepted November 11, 2024

Abstract: In this work, iron oxide nanoparticles (IONPs) were synthesized using green methods. The structural morphological and optical properties of nanoparticles (NPs) were investigated by scanning electron microscopy (SEM), X-ray diffraction (XRD), ultraviolet–visible spectroscopy, and Fourier transform infrared spectroscopy. Based on the SEM analysis, spherical NPs with a size distribution in the range of 50–70 nm were simulated with slight variations in shapes, and the corresponding XRD was calculated. The calculated XRD patterns were then averaged. Well-defined crystalline structure of a single-phase spinel structure and a spherical shape of IONPs were observed. The *in vitro* and *in vivo* biological activities of IONPs synthesized with the hydroalcoholic extract of *Euphorbia milii*'s aerial parts were studied. The antibacterial effects were evaluated against *Staphylococcus aureus*, and the enzyme inhibitory effects of the IONPs and *E. milii* extract on various enzymes were assessed. The IONPs demonstrated significant inhibitory activity against urease (89.09% inhibition), α-glucosidase (72.87% inhibition), carbonic anhydrase II (87.09% inhibition), and xanthine oxidase (85.09% inhibition). The *E. milii* extract also exhibited considerable inhibition of these enzymes. The IC_{50} values for urease, α-glucosidase, carbonic anhydrase II, and xanthine oxidase inhibition by IONPs were 26.09, 59.09, 0.18, and 7.71 μg·mL^{-1}, respectively. The anticancer activity of the IONPs and crude extract was also evaluated. The minimum IC_{50} values were recorded against MDR 2780AD, i.e., 0.85 (extract) and 0.54 (IONPs). Both of the tested samples were found to be significant ($p < 0.001$) analgesic and anti-inflammatory. In contrast, the IONPs were found sedative at all tested doses, and the extract showed a significant ($p < 0.01$) sedative effect at higher doses only.

Keywords: IONPs, *E. milii*, antibacterial activities, enzyme inhibitions, anticancer activities, green synthesis

1 Introduction

Iron oxide nanoparticles (IONPs) have gained significant attention in various fields due to their unique physicochemical properties and potential applications in medicine, environmental remediation, catalysis, antibacterial activities, and enzyme inhibitory effects [1–5]. Nanoparticles (NPs) serve as promising carriers for drug delivery due to their unique physicochemical properties. Their small size grants them access to biological barriers and tissues that larger drug molecules cannot penetrate, enabling targeted delivery to specific cells or tissues within the body. Additionally, NPs can be engineered to encapsulate drugs, protecting them from degradation and allowing for controlled release over time. This controlled release feature

* **Corresponding author: Abdur Rauf,** Department of Chemistry, University of Swabi, Anbar, 23561, Khyber Pakhtunkhwa, Pakistan, e-mail: abdurrauf@uoswabi.edu.pk, mashaljcs@yahoo.com
* **Corresponding author: Haiyuan Zhang,** Laboratory of Chemical Biology, Changchun Institute of Applied Chemistry, Chinese Academy of Sciences, Changchun, 130022, Jilin, China, e-mail: zhangh@ciac.ac.cn
Zubair Ahmad: Department of Chemistry, University of Swabi, Anbar, 23561, Khyber Pakhtunkhwa, Pakistan
Naveed Muhammad: Department of Pharmacy, Abdul Wali Khan, University Mardan, Mardan, Khyber Pakhtunkhwa, Pakistan
Zuneera Akram: Department of Pharmacology, Faculty of Pharmaceutical Sciences, Baqai Medical University, Karachi, Pakistan
Inam Ud Din: Department of Physics, University of Peshawer, Peshawar, Khyber Pakhtunkhwa, Pakistan

is particularly advantageous in maintaining therapeutic drug levels in the body, reducing the frequency of dosing, and minimizing potential side effects. Moreover, surface modifications of NPs can be tailored to enhance their stability, biocompatibility, and target specificity, further optimizing their efficacy as drug carriers. However, ensuring their biocompatibility and assessing potential cytotoxicity are critical steps in their application for biomedical purposes. Studies have shown that surface modifications and coatings can enhance the biocompatibility of IONPs, reducing adverse effects on cells and tissues [6]. Various methods are used for the synthesis of NPs, but conventional approaches often involve the use of toxic chemicals. Therefore, eco-friendly methods utilizing natural products known as green synthesis are emerging. Green synthesis approaches have emerged as sustainable and eco-friendly methods for the fabrication of NPs utilizing natural sources such as plants [7], algae [8], and microorganisms [9]. One key aspect of green chemistry that our method adheres to is the use of natural extracts as reducing and stabilizing agents for the synthesis of IONPs. By utilizing plant extracts, we minimize the use of harmful chemicals and toxic solvents typically associated with traditional synthesis methods. This approach aligns with the principle of reducing the environmental impact of chemical processes. Additionally, the use of plant extracts as reducing agents helps to minimize waste generation during the synthesis process. Phytofabrication, the use of plant extracts for NP synthesis, has distinct advantages over other biological methods. It is cost-effective and sustainable, utilizing readily available plant materials. Plants produce a variety of phytochemicals that serve as effective reducing and stabilizing agents, allowing for simpler and faster synthesis processes compared to microbial methods, which often require complex culture conditions. Additionally, NPs synthesized through phytofabrication typically exhibit better biocompatibility and lower toxicity, making them safer for biomedical applications [10]. *Euphorbia milii*, commonly known as the "crown of thorns," possesses a rich phytochemical profile and has been utilized in traditional medicine for its therapeutic properties [11,12]. The aerial parts of *E. milii*, including leaves and stems, have shown promising bioactive constituents, making them a potential source for NP synthesis with enhanced antibacterial, enzyme inhibitory, and anticancer activities [13,14]. In recent years, there has been growing interest in the green synthesis of IONPs using plant extracts as reducing and stabilizing agents [15,16]. Using plant extracts offers several advantages, including cost-effectiveness, ease of extraction, and reduced use of toxic chemicals [17]. Shen et al. prepared ZnO NPs using *E. milii* as reducing and stabilizing agents, evaluated their antinociceptive, muscle relaxant, and sedative activities, and found significant results [18]. Similarly, Bawazeer also synthesized Ag NPs using extract *E. milii* and evaluated its antibacterial and enzyme inhibitory potential [19]. Furthermore, the biological properties of plant extracts can be harnessed to enhance the therapeutic potential of IONPs [20]. *E. milii*, with its diverse phytochemical composition, possesses inherent antibacterial compounds that can contribute to synthesizing antibacterial IONPs [21]. The antibacterial activities of NPs have gained significant importance in combating bacterial infections and addressing the issue of antibiotic resistance. The unique properties of IONPs, such as their high surface area-to-volume ratio and surface reactivity, enable effective interactions with bacterial cells, leading to bactericidal or bacteriostatic effects [6,22]. The green synthesis of IONPs using *E. milii* extract offers a sustainable and environmentally friendly approach to enhance their antibacterial properties.

Moreover, the biological activities of NPs, particularly their enzyme-inhibitory properties, have been extensively investigated due to their potential therapeutic applications [23]. There exists an unexplored potential in harnessing the unique activities of *E. milii* extracts to enhance NP-mediated drug delivery systems. Despite the documented enzyme inhibition activities of NPs targeting urease, α-glucosidase, carbonic anhydrase II, and xanthine oxidase [24]. Urease enzymes help bacterial infections in the urinary tract to establish themselves in human beings [25]. α-Glucosidase is also an important enzyme involved in the treatment of diabetes [26]. The carbonic anhydrase II has multiple applications in curing osteoporosis [27]. Xanthine oxidase inhibitors, for example, allopurinol used for the treatment of gout and hyperuricemia [28]. Inhibition of these enzymes can lead to potential therapeutic effects, such as anti-diabetic, anti-inflammatory, and anticancer activities. The integration of *E. milii* extract with NPs presents an opportunity to capitalize on the plant extract's inherent properties for improved drug delivery. Although previous works have used *E. milii* extracts for synthesizing other types of NPs like ZnO and Ag NPs, their use in synthesizing IONPs remains underexplored, particularly with regard to their enzyme inhibitory effects and anticancer activities. Moreover, while there is substantial evidence of the antibacterial properties of IONPs, few studies have comprehensively investigated their potential for enzyme inhibition against critical targets like urease, α-glucosidase, carbonic anhydrase II, and xanthine oxidase using *E. milii* extracts. This study aims to fill this gap by utilizing the hydroalcoholic extract of *E. milii* for the green synthesis of IONPs, examining their structural and biological properties, and assessing their potential as biocompatible therapeutic agents in drug delivery and enzyme inhibition. This research aims to synthesize IONPs using hydroalcoholic

extract of *E. milii* and to investigate the *in vitro* and *in vivo* biological activities, including antibacterial effects and enzyme inhibition, anti-inflammatory, sedative, as well as anticancer potential of green synthesized IONPs generated with the crude extract of the aerial parts of *E. milii*. By leveraging the unique activities and properties of *E. milii* extracts, we aim to develop biocompatible and efficient therapeutic agents and drug delivery systems capable of targeted delivery and controlled release of therapeutic agents.

2 Materials and methods

2.1 Plant collection and extraction

The *E. milii* plant was collected from the Tehsil Lahor Distract Swabi Pakistan. The plant was identified by a well-known taxonomist, Dr. Muhammad Ilyas, Assistant Professor at the Department of Botany, University of Swabi, KP, Pakistan. The voucher specimen number UOS/Bot-110 was deposited in the herbarium of the mentioned Department. For the extraction, the 50 g dried plant was ground using a grinder. After grinding, 20 g of the ground plant material (powdered) was introduced into a 200 mL aqueous-methanolic system (8:2) allowing it to be extracted for 1 week [29]. The resulting mixture was then filtered to obtain a clear extract. The filtrate was concentrated using a rotary evaporator to remove the solvent and obtain a concentrated extract. The concentrated extract was subsequently dried using a water bath to evaporate the remaining solvent and obtain a dry extract. The final extract was carefully collected and stored in the refrigerator for future use, ensuring the preservation of its bioactive components.

2.2 NP synthesis

Initially, solutions of 0.1 M $FeCl_3$ and 0.05 M $FeSO_4$ were prepared by dissolving each in distilled water. After mixing both salt solutions, the total volume was brought to 50 mL. Subsequently, 50 mL of the 1% plant extract was added slowly to the salt solutions. 10 mL of Ammonium hydroxide was then added gradually to adjust the pH to approximately 10–12. The solution was stirred for 1–2 h at room temperature, resulting in the formation of a black precipitate, indicating the successful synthesis of Fe_3O_4 NPs. The formation of IONPs was confirmed by monitoring changes in the color of the reaction mixture and analyzing the ultraviolet (UV)–visible (Vis) spectra in the range of 250–750 nm using a UV–Vis spectrophotometer. The NPs were separated from the solution using a magnet, allowing for easy removal from the reaction mixture. The resulting NPs were washed several times with distilled water to remove any unreacted substances. Finally, the purified NPs were dried either in an oven at temperature (around 60°C) to obtain the desired IONPs.

2.3 Instrumentations

A combination of techniques was employed to characterize the IONPs, providing a comprehensive understanding of their morphological features, elemental composition, and chemical interactions. The morphology of the IONPs was visualized using a field emission scanning electron microscopy (SEM) instrument (JEM 2100, Jeol CRL), while elemental analysis was performed using an energy-dispersive X-ray spectroscopy (EDS) instrument (ADX-8000 MINI). To identify the functional groups present in the extract and their interaction with Fe ions during the green synthesis process, the Fourier transform infrared (FTIR) spectrophotometer instrument (Shimadzu FTIR – 8400-S) was utilized. This spectroscopic technique allowed for analyzing the absorption bands and identifying chemical bonds. The time-dependent UV–Vis spectroscopy (300 Plus Optima Japan) was employed to study the formation of IONPs over time. This technique enabled the measurement of changes in the optical properties of the NPs during the synthesis process.

2.4 *In vitro* screening

2.4.1 Antibacterial activity

The antibacterial activity of the synthesized IONPs was assessed against the clinically isolated pathogenic bacterium *Staphylococcus aureus* using the agar well diffusion method [30–32]. Sterile agar plates were prepared, and wells were created using a sterile cork borer. A standardized suspension of *S. aureus* was spread uniformly on the Muller Hinton Agar surface. Subsequently, 50 µL of the synthesized IONP solution was added to the wells. The plates were then incubated at 37°C for 24 h, allowing the diffusion of the IONPs into the agar medium. The experiment involved a negative control using distilled water and a positive control utilizing the standard antibiotic drug linezolid. After the incubation period, the inhibition zones surrounding the wells were measured to evaluate the antibacterial activity of the IONPs. This experiment was performed in triplicate to ensure reliable and reproducible results.

2.4.2 Enzyme inhibitory activities

2.4.2.1 Urease activity

The inhibitory activity of the synthesized IONPs and *E. milii* extract against jack bean urease was assessed. The assay involved incubating 25 µL of jack bean urease, 55 µL of buffer containing 100 mM urea, and 5 µL of the test sample at 30°C for 15 min in 96-well plates. Ammonia production, indicative of urease activity, was determined using the indophenol method. A mixture of 45 µL of phenol reagent (1% w/v phenol and 0.005% w/v sodium nitroprusside) and 70 µL of alkali reagent (0.5% w/v NaOH and 0.1% active chloride NaOCl) was added to each well. After 50 min, absorbance at 630 nm was measured using a microplate reader. The experiment was conducted in triplicate with a final volume of 200 µL. Thiourea was used as a control. The percentage inhibition was calculated using the formula [33]:

$$\text{Percent effect} = 100 - \frac{\text{OD test well}}{\text{OD control}} \times 100$$

2.4.2.2 α-Glucosidase activity

The inhibitory activity of the *E. milii* extract and synthesized IONPs against α-glucosidase was determined. The assay involved the use of *p*-nitrophenyl-α-D-glucopyranoside as the substrate. The absorbance was measured at 405 nm to assess the enzymatic activity in the presence and absence of the IONPs. A standardized solution of α-glucosidase was prepared, and 10 µL of this solution was added to the reaction mixture containing the substrate and various concentrations of the IONPs. The reaction mixture was incubated at the optimal temperature for α-glucosidase activity. After the incubation period, the absorbance was measured using a microplate reader. The percentage inhibition of α-glucosidase by the IONPs was calculated. The experiment was performed in triplicate to ensure accuracy and reproducibility [34].

2.4.2.3 Carbonic anhydrase II enzyme activity

The inhibitory effect of the synthesized IONPs on carbonic anhydrase II enzyme activity was evaluated. The assay involved measuring the hydration of carbon dioxide using a pH indicator. The reaction mixture comprised the test sample (IONPs), the carbonic anhydrase II enzyme, and the substrate. The reaction was performed at the optimal temperature and pH for the enzyme activity. After incubation, the change in pH was measured using a pH indicator. The percentage inhibition of carbonic anhydrase II enzyme activity by the IONPs was calculated, comparing the pH change in the presence and absence of the NPs. The experiment was conducted in triplicate to ensure accurate and reliable results [35].

2.4.2.4 Xanthine oxidase activity

The inhibitory potential of the synthesized IONPs against xanthine oxidase was evaluated using a hydroxylation reaction of xanthine as the substrate, forming colorless uric acid as the end product. The absorbance of uric acid was measured at 296 nm. The reaction mixture included the test sample (IONPs), phosphate buffer, and xanthine oxidase enzyme. A 10 µL test sample solution was prepared, and was dissolved in dimethyl sulfoxide (DMSO). Furthermore, 0.003 units of xanthine oxidase enzyme were disbanded in 20 µL of phosphate buffer, and 20 µL of xanthine ($0.1\ \text{mmol}\cdot\text{L}^{-1}$) was used as the substrate. After adding xanthine oxidase, the mixture was incubated for 10 min at room temperature. Following incubation, the mixture was analyzed in the UV region (λ max 295 nm). Subsequently, the substrate was added, and absorbance readings were recorded at 1-min intervals for 15 min using a microplate reader. The percentage inhibition of the test sample (IONPs) was calculated. The absorbance (A) was calculated using the formula $A = a\lambda \times b \times c$, where $a\lambda$ is the absorptivity coefficient at the specific wavelength, b is the path length, and c is the concentration of the analyte. The IC_{50} values of the compounds were calculated using EZ-Fit Windows-based software. Allopurinol was used as a positive control, and the inhibitory activities of the test samples were compared with the standard. The experiment was performed in triplicate [36].

2.4.2.5 Anticancer activity

Utilizing the MTT assay, the cytotoxicity of the NPs was evaluated [37,38]. RPMI 1640 medium from Gibco BRL was supplemented with 10% fetal bovine serum (Gibco, Institute of Bioinformatics, National Chiao-Tung University, Hsinchu, Taiwan), $100\ \mu\text{g}\cdot\text{mL}^{-1}$ streptomycin sulfate, and $100\ \mu\text{g}\cdot\text{mL}^{-1}$ penicillin sodium salt. In the manufactured media, the human A498 (renal), human hepatoma (HepG2), NCI-H226 (non-small-cell lung), and MDR human ovarian cancer 2780AD cell lines were maintained. Hepatocytes from mice were maintained in 96-well plates. After 48 h, cells were eliminated without treatment, treated with compounds (1.5–100 M), or treated with a vehicle (0.2% DMSO). It was monitored using a 3-[4,5-dimethylthiazol-2-yl]-2,5-diphenyltetrazolium bromide (MTT) assay (Sigma, St. Louis, MO, USA). The remaining cell lines were also subjected to an identical assay. The concentration–effect curves were utilized to calculate the IC_{50} of the test chemical across several cell lines. Paclitaxel (Sigma) was used as a positive due to its well-established cytotoxic effects across a wide range of cancer cell lines. As a widely used chemotherapeutic agent, paclitaxel serves as a benchmark for assessing the cytotoxic potential of novel compounds or formulations in cancer research. *In vitro*,

cytotoxicity testing was conducted on LCMK-2 chimpanzee kidney epithelial cells and mouse hepatocytes. After 24 h of incubation, cell viability was determined using MTT assays. The cells were maintained in 10% fetal bovine serum (Gibco BRL), 2 mg·mL^{-1} of sodium bicarbonate solution, 110 g·mL^{-1} of penicillin sodium salt, and 100 g·mL^{-1} of streptomycin sulfate (all from RPMI 1640) medium. In the first image, 7.1 × 10^3 LCMK-2 cells and 8.6 × 10^3 murine hepatocytes were seeded into 96-well plates. After 48 h of incubation, cell viability was determined using the MTT method (Sigma) with or without vehicle (0.2% DMSO).

2.5 *In vivo* screening

2.5.1 Animals

Healthy BALB/c mice having a weight range from 23 to 28 g were obtained from the National Institute of Health Islamabad, Pakistan. The animals were kept under standard laboratory conditions mentioned in animals' laws approved ethical committee (SOU/Pharm-23) of the Pharmacy Department University of Swabi, KPK, Pakistan. The animals were fed with standard laboratory food and environmental conditions, i.e., with 12/12 dark and light cycle. All the animals were allowed to drink water and take food *ad libitum*.

2.5.2 Analgesic screening

Using a hot plate analgesia meter, the progression of the analgesic effect was monitored. As such, the animals were categorized into negative control (normal saline, 10 mL·kg^{-1}), positive control (Tramadol 10 mg·kg^{-1}), and tested groups (n = 8). Across the board, the animals' reactions to heated surfaces were measured. After administering the extract and NPs to the animals for 30 min, the latency time (the time required for jumping of animal) was measured in seconds. The animal whose staying duration exceeded 25 s (cut-off time) was excluded from the analysis. On multiple occasions (30, 60, 90, and 120 min after treatment), the latency time was measured. The preferred medication considered a standard drug was tramadol [39].

2.5.3 Sedative screening

Our previously published paradigm [40] was used to evaluate the sedative effect of the extract and NPs using the open-field method. The soundproofing of the experiment chamber consisted of a wooden cage with equal space. The animals were categorized (n = 8) as described previously, and diazepam (0.5 mg·kg^{-1}) was administered to the positive control group. After 30 min of treatment with normal saline (negative control), diazepam (positive control), and extract/IONPs (testing groups), the sedative effect of each animal in the unique wooden cage was assessed. The animal was placed in the center of the cage, and the number of lines it crossed was recorded for 10 min. The substance is less sedative, the greater the number of crossed lines, and *vice versa*.

2.5.4 Anti-inflammatory activity

Carrageenan-induced paw edema was used for evaluation of the anti-inflammatory effect. The animals were classified as the above grouping (n = 8). The normal saline was administered to the animals in the negative control group, while the diclofenac sodium was issued to the positive control group. The remaining groups received the extract and IONPs as treatment. After these treatments had been administered for 30 min, each animal's right hind paw was injected subcutaneously with carrageenan (1%, 0.05 mL). It was determined that the hand swelled due to the induced inflammation. At regular intervals, the volume of this limb was measured, and the percentage of inflammation reduction was calculated [41].

2.6 Statistical analysis

The results obtained in this investigation are given the mean ± standard error of the mean to obtain the significant difference (p < 0.05 or 0.01). The statistical analysis was done with the help of GrapPad Prism.

Ethical approval: The research related to animals' use has been complied with all the relevant national regulations and institutional policies for the care and use of animals. The animals were kept under standard laboratory conditions mentioned in animal laws approved by the ethical committee (UOS/Pharm-23) of the Pharmacy Department University of Swabi, KP, Pakistan.

3 Results

3.1 Sythesis and characterizations

3.1.1 UV–Vis spectroscopy

UV–Vis spectroscopy characterized the synthesized IONPs. A solution of 3 mL of IONPs was taken in cuvette, and its

spectrum was recorded using a UV–Vis spectrophotometer. The absorption peak at 295 nm (λ max) was observed, indicating the presence of IONPs (Figure 1) [42,43]. The UV–Vis spectra provided valuable information regarding the optical properties and the absorbance of the IONPs at a specific wavelength. This analysis confirmed the successful synthesis of IONPs in the solution.

3.1.2 FTIR spectroscopy

FTIR spectroscopy plays a crucial role in identifying functional groups present in compounds. This study recorded the FTIR spectra for the *E. milii* plant extract and the synthesized IONPs to analyze their respective functional groups. The FTIR spectra of both IONPs and the plant extract exhibited several typical peaks, indicating the presence of similar functional groups. A prominent broad peak at 3,406 cm^{-1} was observed in the plant extract and IONPs, suggesting O–H stretching vibrations from alcohol or phenolic groups. Notably, the broadness of this peak in the IONPs was slightly weaker compared to the plant extract, suggesting potential modifications in hydrogen bonding or interactions of the functional groups upon forming IONPs. Another shared feature was a small peak at 2,044 cm^{-1}, corresponding to the stretching vibrations of C≡N groups, indicating the presence of nitrile functional groups.

Additionally, a sharp peak at 1,628 cm^{-1} was observed in both the plant extract and IONPs, attributed to the stretching vibrations of C═O bonds, indicating the presence of carbonyl groups. In the plant extract, additional small peaks at 1,377 and 1,257 cm^{-1} were observed, corresponding to C–H bending vibrations and C–O stretching vibrations, respectively. However, in the IONPs, the intensity of these peaks changed, suggesting potential interactions or adsorption of these functional groups on the NP surface. Interestingly, an exclusive sharp and narrow peak at 1,016 cm^{-1} was observed in the FTIR spectrum of IONPs. This could be attributed to the stretching vibrations of metal–oxygen bonds, providing evidence for forming IONPs. The FTIR spectrum of the plant extract and IONPs is shown in Figure 2.

3.1.3 SEM analysis

SEM analysis was performed to examine the morphology of the synthesized NPs. The sample was prepared by placing a drop of the synthesized IONPs on a suitable substrate and allowing it to dry. The SEM analysis shows the presence of both spherical and irregular-shaped particles and can be attributed to the complex nature of the synthesis process, which can lead to variations in particle morphology. Factors such as reaction kinetics, precursor concentration, and temperature gradients within the reaction vessel can influence the final shape of the NPs. Additionally, the rough background matrix may result from the presence of residual reactants or other byproducts from the synthesis process. High-resolution SEM images were captured at various magnifications to observe the NPs' surface details and size distribution. Additionally, low-resolution SEM images were recorded to provide an overview of the morphology and assess the NPs' uniformity. The SEM analysis confirmed the successful formation of spherical IONPs, as depicted in Figure 3.

Information from SEM images is used to simulate IONPs through the DISCUS package. The spherical shape

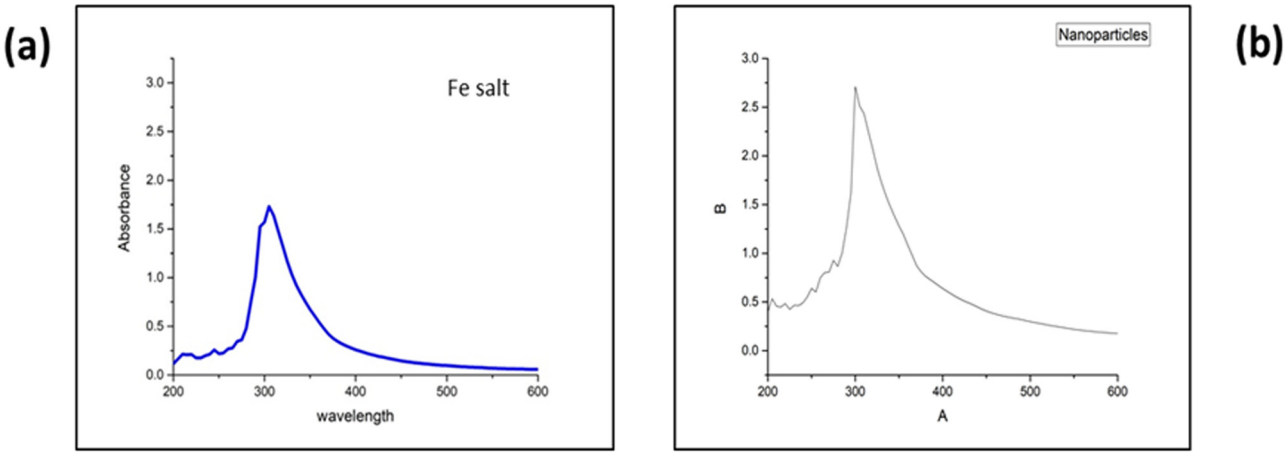

Figure 1: UV–Vis, spectra of the iron salt (a) and biosynthesized IONPs (b).

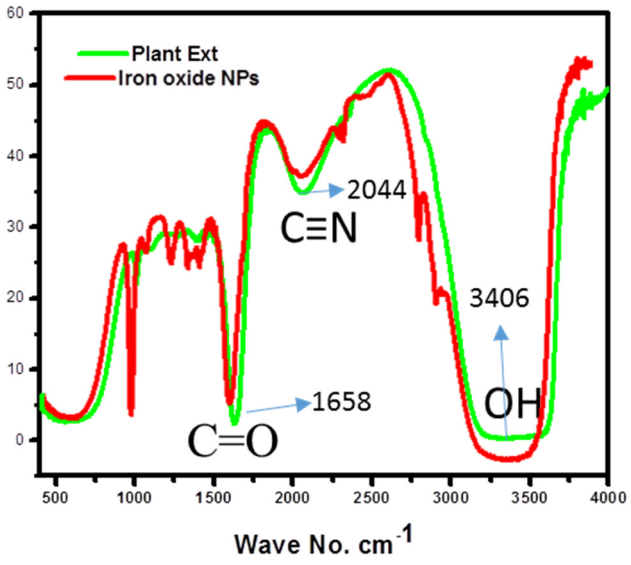

Figure 2: *E. milii* ext and IONP FTIR spectra.

of IONPs is shown in Figure 4. The average size of the synthesized NPs obtained from SEM images and the simulated spherical shape suggest a particle distribution ranging from 50 to 70 nm. The synthesized NPs' average size from SEM images and simulated spherical shape suggest the particle distribution of various sizes ranging from 50 to 70 nm.

3.1.4 X-ray diffraction (XRD)

In this study, we investigated the XRD patterns of our prepared samples within the 2θ range of 20°–100° at room temperature. To enhance visualization, the pattern was further scaled down from 20° to 80° The crystalline nature of the synthesized samples was confirmed by the remarkable peak intensities, while the broad full width at half maximum (FWHM) indicates the formation of nano-sized particles, as depicted in Figure 5. Notably, no impurity peaks or other phases associated with IONPs were observed, demonstrating the exceptional phase purity of our synthesized NPs. The lattice constant was determined using XRD data. The following relation was to determine the *d*-spacing and the lattice parameter (a) for cubic structure,

$$d_{hkl} = \lambda/(2 \sin \theta)$$

$$a = d_{hkl} \times (h^2 + k^2 + l^2)^{0.5}$$

where d_{hkl} represent the interplanar spacing, λ is the wavelength of the incident X-ray, and θ is known as Bragg's angle.

The results show a lattice parameter of 8.3912 Å and in close agreement with entry number mp-19306 (a = 8.44397 Å) at the open database material project [44]. For accurately estimating the crystallite/NP size, a pseudo-Voigt function ($P{\cdot}V(x;f)$ was fitted to the XRD data,

$$(P \cdot V\ (x;f) = \ \eta \cdot G(x,f) + (1 - \eta) \cdot L(x,f))$$

where G, L, and η correspond to Gaussian, Lorentzian, and peak profile parameters and are applied to well-resolved diffraction peaks in the XRD data. The FWHM obtained from the fitting process was then used in the Debye–Scherrer equation, $D = K\lambda/\beta \cos \theta$, where D represents the particle size, K is a constant (0.9 for spherical NPs), λ is the wavelength of the X-ray used, β is the FWHM in radians, and θ is the diffraction angle. The estimated particle size of the IONPs calculated from XRD analysis is approximately in the range of 36–47 nm.

3.2 Crystal structure

Fe_3O_4 has a spinel structure that belongs to the cubic crystal system and exhibits remarkable properties with various applications. The crystal structure is shown in

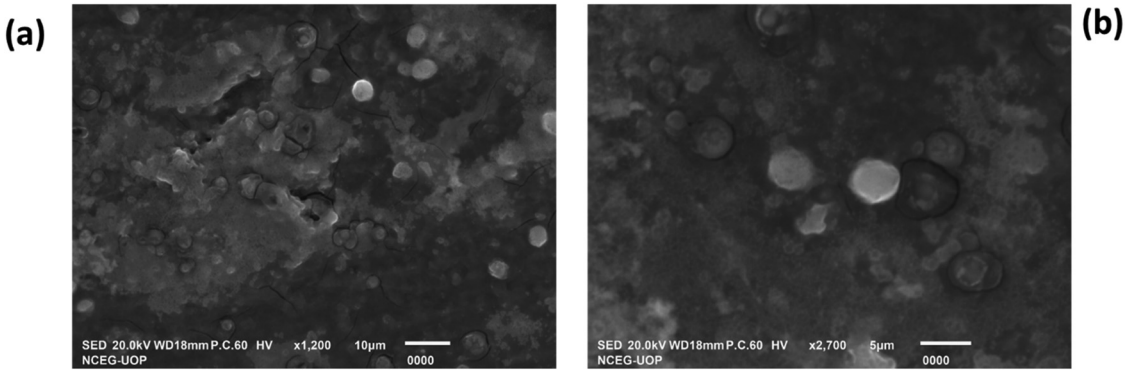

Figure 3: SEM images of IONPs. Low resolution (a) and high resolution (b).

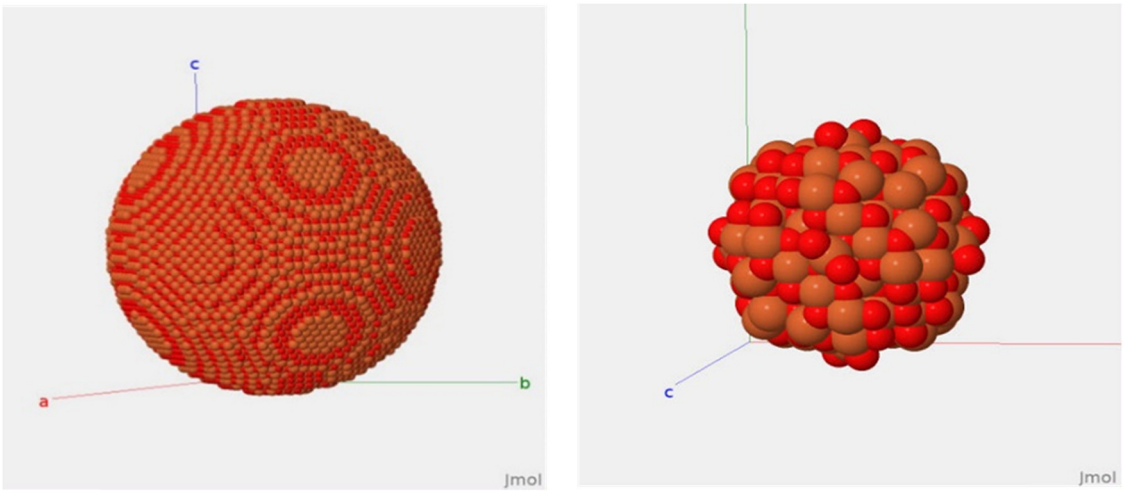

Figure 4: Simulated spherical structure of IONPs.

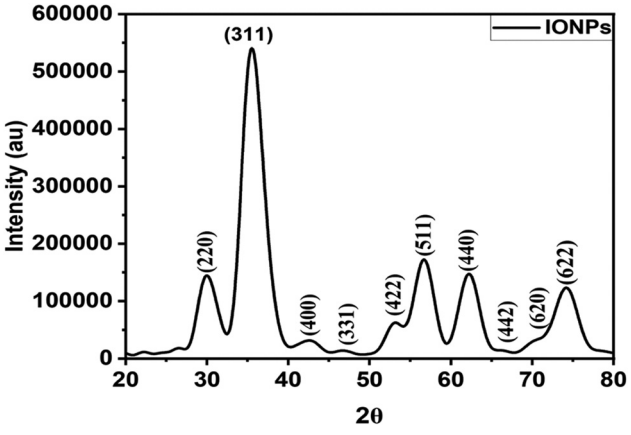

Figure 5: XRD of synthesized IONPs.

Figure 6: lattice parameters a, b, and c = 8.44397 Å and angles α, β, and γ = 90°. Fe_3O_4 crystal lattice comprises Fe^{2+} and Fe^{3+} ions bonded to oxygen O^{2-} atoms. The arrangement involves Fe_3O_4 tetrahedra, where each Fe^{2+} ion is bonded to four O^{2-} atoms, sharing corners with twelve Fe_3O_4 octahedra, in which each Fe^{3+} ion is bonded to six O^{2-} atoms. The Fe–O bond lengths are 1.92 Å for Fe^{2+} ions and 2.06 Å for Fe^{3+} ions. The unique bonding arrangement and the cubic symmetry contribute to the distinct properties and applications of Fe_3O_4 and other Spinel-based materials [45].

The spinel crystal structure of IONPs offers unique advantages for antibacterial and inhibitory effects. Its high surface area-to-volume ratio enables enhanced interactions with bacterial cells, promoting effective antibacterial activity. The stable arrangement of iron and oxygen ions in the spinel structure ensures prolonged efficacy. The nanoscale size allows IONPs to penetrate bacterial cells, leading to membrane disruption and inhibition of bacterial growth. Additionally, their ability to induce oxidative stress enhances their antibacterial properties. Furthermore, IONPs' unique crystal structure facilitates functionalization for targeted drug delivery, reducing resistance development and minimizing adverse effects on healthy cells. These properties make IONPs with the spinel crystal structure promising candidates for biomedical applications.

3.2.1 EDS

The EDS analysis investigated the elemental composition of the green-synthesized IONPs derived from *E. milii* extract. The EDS analysis revealed the presence of several elements. Carbon and oxygen were found to be the major constituents, comprising approximately 20% and 17.54% of the composition,

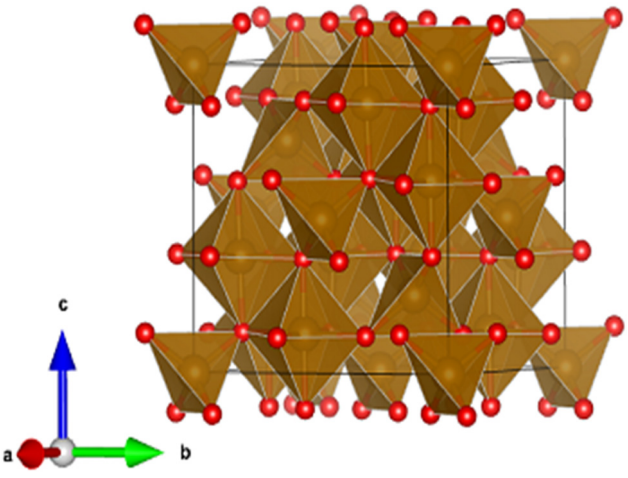

Figure 6: Fe_3O_4 crystal structure.

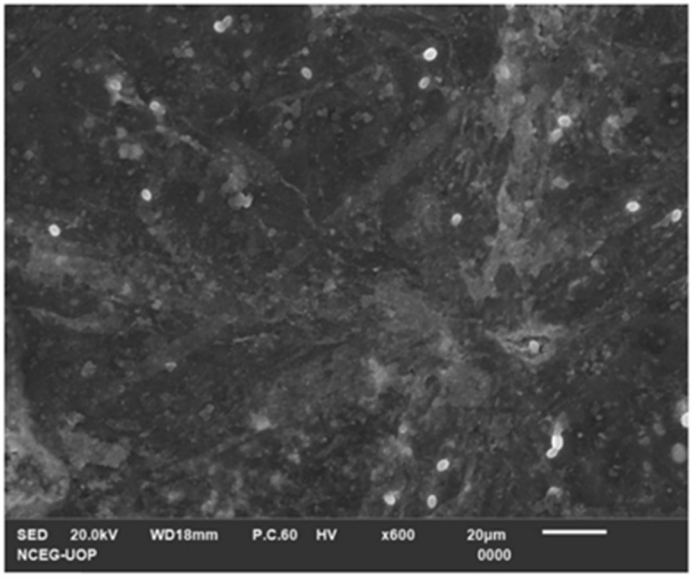


```
Volt            : 20.00 kV
Mag.            : x 600
Date            : 2023/04/19
Pixel           : 1280 x 960

Acquisition Condition
Instrument      : IT100LA
Volt            : 20.00 kV
Current         : ---
Process Time    : T4
Live time       : 16.51 sec.
Real Time       : 17.88 sec.
DeadTime        : 7.00 %
Count Rate      : 4900.00 CPS
```

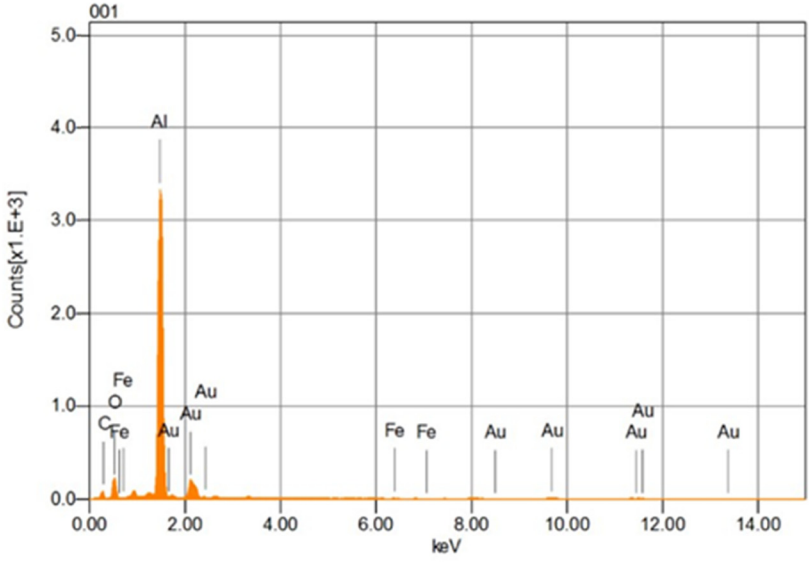

Formula	mass%	Atom%	Sigma	Net	K ratio	Line
C	20.80	37.64	0.10	2334	0.0010699	K
O	17.54	23.83	0.17	5444	0.0114042	K
Al	44.61	36.74	0.19	127601	0.0834124	K
Fe	1.09	0.03	0.05	73	0.0001567	K
Au	15.96	1.76	0.30	12687	0.0153723	M
Total	100.00	100.00				

JEOL EDS System JEOL

Figure 7: EDS spectrum of the synthesized IONPs.

respectively, as shown in the inset of Figure 7. The identification of carbon and oxygen suggests the involvement of organic compounds, potentially derived from biomolecules present in the extract. Notably, the analysis confirmed the successful synthesis of IONPs, as a minor quantity of iron (1.09%) was observed. These results underscore the potential role of organic compounds from the extract in reducing iron ions and subsequent NP synthesis.

3.3 *In vitro* biological activities

3.3.1 Antibacterial activity assessment

The experiment involved a negative control using distilled water, a positive control utilizing the standard antibiotic drug linezolid, and an additional control utilizing the *E. milii* extract without IONPs. The agar well diffusion method results demonstrated the inhibitory effects of the linezolid antibiotic and the synthesized IONPs against *S. aureus*. The zone of inhibition calculated for linezolid indicating its potent antibacterial activity. Similarly, the IONPs displayed significant antibacterial activity, with a zone of inhibition measuring 21.45 mm. These results highlight the promising antibacterial properties of the synthesized IONPs. The antibacterial effect of both tested samples and their mechanistic diagram is presented in Figure 8 and Table 1. The zone of inhibition against tested microorganisms was 21.45 (NPs) and 17.67 (extract).

Table 1: Antibacterial activity assessment of IONPs against *S. aureus* and comparison with previously reported literature

Sample	Zone of inhibition (mm)	Reference
Linezolid	25.98 ± 1.34	This work
IONPs	21.45 ± 1.34	
E. milii extract	17.67 ± 1.34	
Distilled water (control)	—	
Ag NPs derived from *E. milii*	20	[19]
IONPs prepared via co-precipitation	13.8	[46]
IONPs synthesized from *Lagenaria siceraria*	8	[20]

3.3.2 Enzyme inhibition assessment

Enzyme inhibition assays were performed to evaluate the inhibitory effects of the *E. milii* extract, and IONPs were tested on four different enzymes: urease, α-glucosidase, carbonic anhydrase II, and xanthine oxidase. The percentage inhibition and IC_{50} values were determined to assess the potency of the inhibitory activity.

3.3.3 Effect on urease

The urease inhibition assay revealed significant inhibitory effects of the *E. milii* extract and IONPs. The *E. milii* extract exhibited 70.21% inhibition at a concentration of 0.2 $\mu g \cdot mL^{-1}$. In comparison, the IONPs demonstrated enhanced inhibition, with a remarkable percentage of 89.09% at a concentration of 0.25 $\mu g \cdot mL^{-1}$. These results indicate that the IONPs derived from the *E. milii* extract possess potent inhibitory activity against urease. Thiourea used as a positive control, exhibited potent inhibition of 99.01%, validating the assay's effectiveness as shown in Table 2.

3.3.4 Effect on α-glucosidase

The α-glucosidase inhibition assay demonstrated considerable inhibitory effects of the *E. milii* extract and IONPs. The

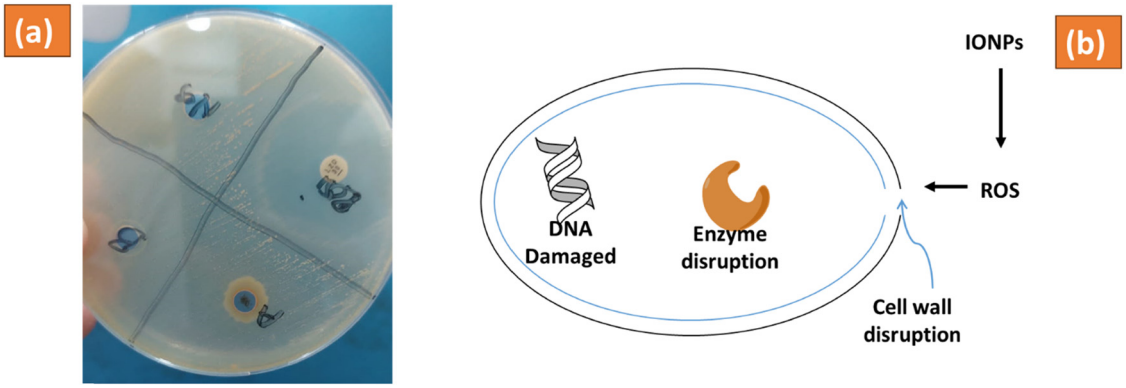

Figure 8: Antibacterial activity assessment of IONPs (a) and mechanistic diagram (b) of *E. milii* IONPs against *S. aureus*.

E. milii extract displayed 43.09% inhibition at a concentration of 0.2 μg·mL^{-1}. In contrast, the IONPs exhibited increased inhibitory activity, with a percentage of 72.87% at a concentration of 0.25 μg·mL^{-1}. These results indicate that the IONPs derived from the *E. milii* extract possess notable inhibitory activity against α-glucosidase. Acarbose, the positive control, exhibited a high inhibition percentage of 97.45%, further confirming the efficacy of the assay as described in Table 2.

3.3.5 Effect on carbonic anhydrase II enzyme

The carbonic anhydrase II enzyme inhibition assay demonstrated significant inhibitory effects of the *E. milii* extract and IONPs. The *E. milii* extract exhibited 72.32% inhibition at a concentration of 0.2 μg·mL^{-1}, while the IONPs demonstrated enhanced inhibitory activity with a percentage of 87.09% at a concentration of 0.25 μg·mL^{-1}. Remarkably, the IONPs exhibited an IC_{50} value of 0.18 ± 0.05 μg·mL^{-1}, indicating their high potency in inhibiting carbonic anhydrase II enzyme activity. Acetazolamide, the positive control, displayed a substantial inhibition percentage of 90.65%, validating the accuracy of the assay as shown in Table 2.

3.3.6 Effect on xanthine oxidase

The xanthine oxidase inhibition assay revealed significant inhibitory effects of the *E. milii* extract and IONPs. The *E. milii* extract exhibited 77.32% inhibition at a concentration of 0.2 μg, while the IONPs demonstrated enhanced inhibitory activity with a percentage of 85.09% at a concentration of 0.25 μg·mL^{-1}. Notably, the IONPs exhibited an IC_{50} value of 7.71 ± 0.06 μg·mL^{-1}, highlighting their strong inhibitory potential against xanthine oxidase activity. Allopurinol, the positive control displayed a remarkable inhibition percentage of 98.02%, as shown in the inset of Table 2.

3.3.7 Anticancer activity

The efficacy of the extract and synthesized IONPs from *E. milii* in combating cancer was evaluated against various cancer cell lines, with results presented in Table 3. Notably, the minimum IC_{50} values were observed against the MDR 2780AD cell line, demonstrating potent anticancer effects with IC_{50} values of 0.85 μg·mL^{-1} for the extract and 0.54 μg·mL^{-1} for the NPs. Table 3 provides a comprehensive overview of the in-vitro anticancer screening results. The extract exhibited moderate anticancer activity across the tested cell lines, with IC_{50} values ranging from 57.09 μg·mL^{-1} (HepG2) to 111.65 μg·mL^{-1} (NCI-H226). Similarly, the synthesized IONPs demonstrated variable efficacy, with IC_{50} values ranging from 15.98 μg·mL^{-1} (HepG2) to 65.87 μg·mL^{-1} (NCI-H226). Comparison with the positive control, paclitaxel, reveals that both the extract and NPs exhibit comparable anticancer activity against certain cell lines. These findings suggest that the extract and synthesized IONPs from *E. milii* possess promising anticancer properties, particularly against the MDR 2780AD cell line.

3.4 *In vivo* screening

3.4.1 Analgesic effect

The analgesic effect of both of the tested samples is demonstrated in Table 4. A dose-dependent and time-dependent

Table 2: Enzyme Inhibitory screening of extract and Iron oxide NPs from *E. milii*

Enzyme	Tested samples	Concentrations	% inhibition	IC_{50}
Urease	*E. milii*	0.2 μg·mL^{-1}	70.21	31.05 ± 1.32 μg·mL^{-1}
	IONPs	0.25 μg·mL^{-1}	89.09	26.09 ± 1.65 μg·mL^{-1}
	Thiourea	0.2 μM	99.01	21.98 ± 1.01 μM
α-Glucosidase	*E. milii*	0.2 μg·mL^{-1}	43.09	—
	IONPs	0.25 μg·mL^{-1}	72.87	59.09 μg·mL^{-1}
	Acorbose	0.2 μM	97.45	28.09 ± 1.09 μM
Carbonic anhydrase II enzyme	*E. milii*	0.2 μg·mL^{-1}	72.32	38.01 ± 0.88 μg·mL^{-1}
	IONPs	0.25 μg·mL^{-1}	87.09	0.18 ± 0.05 μg·mL^{-1}
	Acetazolamide	0.2 μM	90.65	0.13 ± 0.03 μM
Xanthine oxidase	*E. milii*	0.2 μg·mL^{-1}	77.32	28.04 ± 0.10 μg·mL^{-1}
	IONPs	0.25 μg·mL^{-1}	85.09	7.71 ± 0.06 μg·mL^{-1}
	Allopurinol	0.2 μM	98.02	2.21 ± 0.02 μM

Values are indicated as mean ± standard error of the mean of three different experiments.

Table 3: *In-vitro* anticancer screening of extract and iron oxide NPs from *E. milii*

Samples	IC_{50}			
	HepG2	A498	NCI-H226	MDR 2780AD
E. milii	57.09 ± 1.23 μg·mL^{-1}	119.76 ± 1.23 μg·mL^{-1}	111.65 ± 1.23 μg·mL^{-1}	0.85 ± 0.12 μg·mL^{-1}
IONPs	15.98 ± 0.65 μg·mL^{-1}	98.87 ± 0.79 μg·mL^{-1}	65.87 ± 0.84 μg·mL^{-1}	0.54 ± 0.09 μg·mL^{-1}
Paclitaxel	7.85 ± 0.54 mM	94.87 ± 0.76 mM	62.86 ± 0.72 mM	0.21 ± 0.07 mM

effect was observed. Both of the tested samples significantly reduced the latency time. The peak significant effect was observed after 60 min of experimental duration and remained significant up to the end of the experimental period. The analgesic effect of NPs was better than extract.

3.4.2 Sedative effect

The sedative effect of extract and NPs is presented in Table 5. The extract demonstrated a significant ($p < 0.01$) sedative effect at the tested dose of 250 mg·kg^{-1}, while the IONPs exhibited significant ($p < 0.001$) sedative at all tested doses.

3.4.3 Anti-inflammatory effect

The anti-inflammatory properties of the extracts and IONPs were assessed, and the results are depicted in Figure 9. Notably, the crude extract displayed significant anti-inflammatory activity, exhibiting 53.00% activity after the third hour and 30.21% activity after the fifth hour. In comparison, the NPs demonstrated robust anti-inflammatory effects, with 90.23% activity after the third hour and 70.12% activity after the fifth hour. Diclofenac was used as a standard drug.

4 Discussion

The green synthesis of NPs stands as a revolutionary approach in nanotechnology, offering numerous advantages over traditional chemical methods. Unlike conventional synthesis routes that often involve hazardous chemicals and energy-intensive processes, green synthesis harnesses the power of nature's resources, such as plant extracts and microbes to fabricate NPs. This eco-friendly approach not

Table 5: *In vivo* sedative screening of extract and IONPs from *E. milii*

Samples	Dose (mg·kg^{-1})	No lines crossed
Control	5 mL	119.00 ± 2.98
Diazepam	0.5	9.20 ± 0.65***
E. milii	25	87.09 ± 2.09
	50	78.09 ± 3.00
	100	69.65 ± 2.65
	250	56.09 ± 64**
IONPs	2.5	40.87 ± 2.09**
	5	31.12 ± 2.76***
	10	20.09 ± 1.99***
	15	10.09 ± 1.98***

The data were analyzed using ANOVA. *** = 0.001 > p, ** = 0.01 > p, * = 0.05 > p.

Table 4: *In vivo* analgesic screening of extract and Iron oxide NPs from *E. milii*

Group	Dose (mg·kg^{-1})	Time duration (min), latency time (s)			
		30	60	90	10
Normal saline	10 mL	10.00 ± 0.08	9.98 ± 0.06	9.98 ± 0.12	9.90 ± 0.11
Tramadol	10	25.23 ± 0.07***	25.30 ± 0.13***	26.00 ± 0.15***	26.43 ± 0.12***
E. milii	10	9.76 ± 2.54	14.65 ± 2.23	15.87 ± 2.09	14.08 ± 1.87
	25	10.21 ± 2.21	16.00 ± 1.98**	17.02 ± 1.96**	17.98 ± 1.87**
	50	12.09 ± 2.16	18.43 ± 2.00**	19.28 ± 1.90**	20.02 ± 2.09***
	100	15.32 ± 1.90*	20.76 ± 2.01**	21.09 ± 2.04***	21.98 ± 2.10***
	250	17.65 ± 1.87**	22.34 ± 1.65***	23.09 ± 1.43***	22.65 ± 2.19***
IONPs	2.5	15.09 ± 1.45*	18.98 ± 1.34**	19.23 ± 1.00**	18.87 ± 1.48**
	5	18.87 ± 1.65**	21.65 ± 1.54***	22.09 ± 1.65***	21.76 ± 1.43***
	10	21.98 ± 1.02**	24.65 ± 1.43***	24.90 ± 1.33***	23.43 ± 1.09***

The data were analyzed using ANOVA. *** = 0.001 > p, ** = 0.01 > p, * = 0.05 > p.

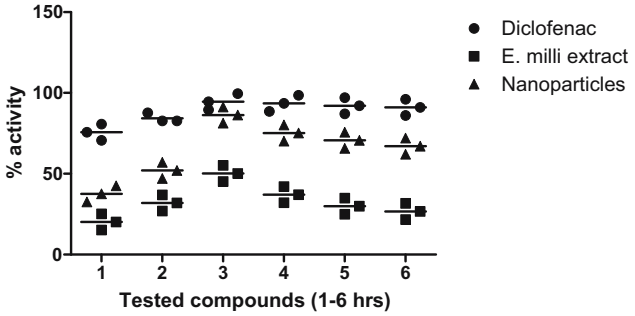

Figure 9: Percent anti-inflammatory activity of extract and iron oxide NPs from *E. milii*.

only minimizes environmental impact but also promotes sustainability by utilizing renewable sources [7]. Furthermore, green synthesis typically operates under mild conditions, reducing energy consumption and minimizing the generation of toxic byproducts. Additionally, the bioactive compounds present in the natural extracts used for synthesis can impart unique properties to the resulting NPs, enhancing their functionality for various applications [47]. Moreover, green synthesis often results in NPs with higher stability, biocompatibility, and uniformity, making them well-suited for biomedical, environmental, and industrial applications. Utilizing the hydroalcoholic extract as a reducing and stabilizing agent provides a natural and eco-friendly approach for NP synthesis with enhanced antibacterial, enzyme inhibitory, anti-inflammatory, analgesic, sedative, and anticancer potential. Moreover, the utilization of plant extracts allows for the incorporation of inherent antibacterial and enzyme-inhibitory compounds, further enhancing the therapeutic potential of the synthesized NPs [48,49]. In this study, we investigated the environmentally friendly synthesis of IONPs using a plant extract from *E. milii* and assessed their various biological activities. The SEM, XRD, UV–Vis spectroscopy, and FTIR spectroscopy were used to characterize the NPs. The IONPs was simulated through the DISCUS package based on the SEM analysis, spherical NPs with a size distribution in the range of 50–70 nm conform slight variation in shapes, and the corresponding XRD was calculated. The spherical symmetry offers several advantages, including an enhanced surface area-to-volume ratio, facilitating increased interaction with the environment. The compact and uniform shape enables efficient cellular uptake, enhancing bioavailability and target cell interaction [50]. Additionally, the spherical form minimizes particle aggregation, leading to improved stability and prolonged activity. Their homogeneous distribution ensures consistent and predictable effects, crucial for anti-bacterial applications. These NPs exhibit strong antibacterial activity due to their small size and uniform shape, allowing effective penetration and disruption of bacterial cells. Furthermore, the spherical symmetry allows precise control in drug delivery, leading to targeted therapy and improved outcomes. With reduced toxicity, especially in well-defined sizes, they show promise in biomedical applications, promoting better biocompatibility and reducing adverse effects on living systems. The calculated XRD patterns were then averaged. Well-defined crystalline structure of a single-phase spinel structure and a spherical shape were IONPs were observed. The stable and spherical surface morphology achieved, along with the unique spinel crystal structure, holds significant importance in enhancing inhibition and antibacterial effects. The possible mechanism of the formation of Fe_3O_4 (magnetite) NPs in our study occurs through a green synthesis mechanism facilitated by the hydroalcoholic extract of *E. milii*. The bioactive compounds present in the plant extract serve as reducing agents, converting ferric ions (Fe^{3+}) to ferrous ions (Fe^{2+}) during the reaction. As the reaction progresses, these ferrous ions aggregate and nucleate, forming small clusters of Fe_3O_4. This nucleation is followed by growth, as additional iron ions deposit onto the clusters, resulting in the formation of larger NPs. The stabilization of these NPs is achieved through the phytochemicals in the extract, such as flavonoids and phenolic compounds, which coat their surfaces and prevent agglomeration, ensuring a uniform size distribution [51]. Subsequently, we set their antibacterial, enzyme inhibitory, anticancer, analgesic, sedative, and anti-inflammatory properties the results showing the successful synthesis of spherical IONPs with unique properties and enhanced biological activities. The UV–Vis absorption peak at 295 nm and the distinctive functional groups seen in the FTIR spectra proved that the synthesis of IONPs had succeeded. The IONPs' uniform and spherical morphology were investigated through SEM analysis. The EDS analysis showed that the plant extract's organic compounds were used to synthesize the NPs. Compared to the plant extract, the IONPs demonstrated enhanced antibacterial activities against *S. aureus*. This is due to the generation of ROS and can be influenced by the surface area charge on nanomaterials [52,53]. They also showed significant inhibition against urease, glucosidase, and carbonic anhydrase II. Their potent anticancer activity, especially against the multidrug-resistant MDR 2780AD cell line, highlights their potential as effective anticancer agents. *In vivo*, screening revealed dose-dependent analgesic and sedative effects and higher anti-inflammatory activity compared to the plant extract. This finding is comparable with the previous studies. Katata-Seru et al. studied the antibacterial activities of green-synthesized iron NPs and found a zone of inhibition of 6 mm against *Escherichia coli* [54]. Similarly, Sivakami et al. also investigated the biological activities, including anti-inflammatory effects

(87% at 500 μg·mL^{-1}), using green-synthesized iron NPs synthesized with *Cinnamomum verum* bark extract [55]. Yusefi et al. screened the green synthesized iron NPs with 2 and 4 wt% of peel extract showed potent anticancer activities (IC_{50} of 197.46 and 85.06 μg·mL^{-1}, respectively) against nasopharyngeal carcinoma cell line [56]. The thriving green synthesis of IONPs using *E. milii* extract presents a sustainable and environmentally friendly approach for producing NPs with diverse biomedical applications. The strong antibacterial and enzyme-inhibitory properties of IONPs point to their potential for treating microbial infections and acting as therapeutic enzyme inhibitors. The potent anticancer activity of IONPs also offers encouraging prospects for targeted cancer therapies, particularly in cases of multidrug resistance. Their potential uses in pain management and inflammatory disorders are further supported by their analgesic, sedative, and anti-inflammatory effects. Bioengineered metallic NPs present significant opportunities in the field of nanomedicine, primarily due to their unique physicochemical properties that enhance drug delivery, imaging, and therapeutic applications, which can enhance therapeutic efficacy while minimizing side effects. However, several challenges remain in the widespread adoption of these NPs in clinical settings. Key issues include potential toxicity, variability in biological responses among different populations, and the need for extensive regulatory approvals. Furthermore, the stability and reproducibility of bioengineered NPs can be affected by environmental factors, raising concerns about their long-term safety and efficacy. Addressing these challenges through thorough research, standardized protocols, and robust safety assessments will be crucial for realizing the full potential of bioengineered metallic NPs in nanomedicine [49].

5 Limitations

The understanding of the mechanisms underlying the biological activities of green-synthesized NPs is still limited, necessitating further research to elucidate their mode of action and potential side effects. While green synthesis reduces environmental impact compared to traditional methods, the overall environmental footprint, including energy consumption and waste generation during extraction and synthesis processes, needs to be carefully evaluated. While our study demonstrates significant biological activities, including potent antibacterial effects, it is important to acknowledge a limitation in the scope of our antibacterial testing. We focused our antibacterial assays solely on *S. aureus* as a representative bacterial strain. However, bacterial species exhibit diverse responses to antimicrobial agents due to variations in cell wall structure, membrane permeability, and resistance mechanisms. Therefore, the observed antibacterial activity against *S. aureus* may not necessarily translate to other bacterial species. This limitation underscores the need for future studies to investigate the broad-spectrum antibacterial efficacy of the synthesized NPs against a range of clinically relevant bacterial pathogens. Exploring the mechanisms underlying the antibacterial activity and potential development of resistance is crucial for the rational design of NP-based antibacterial agents with enhanced efficacy and reduced risk of resistance emergence. We did not investigate the stability of the NPs over time or under different environmental conditions. The stability of NPs is crucial for their practical applications, particularly in fields such as biomedicine, where long-term stability is essential for efficacy and safety. The lack of stability studies in our research prevents us from fully understanding the behavior of the NPs under various conditions and limits the applicability of our findings. Additionally, future studies should delve into stability and the molecular mechanisms of IONPs' biological activities, including their interactions with target molecules and pathways. Long-term toxicity studies and bio-distribution analyses are essential to assess the biocompatibility and safety of IONPs for potential clinical applications. Investigating IONPs' potential in combination therapies, such as their synergistic interactions with currently available antibiotics or chemotherapeutic agents, could improve their therapeutic efficacy and reduce the risk of drug resistance. Additionally, IONPs' applications in personalized medicine and diagnostics may be expanded as research into their potential as imaging or a drug delivery agent continues.

6 Conclusion

In this study, the thriving green synthesis of biocompatible and multifunctional IONPs using *E. milii* extract was demonstrated. The IONPs exhibited a spherical shape with a unique spiral crystal structure and a size distribution ranging from 50 to 70 nm, as characterized by various tools and simulations. These IONPs displayed potent biological activities, including antimicrobial, enzyme inhibitory, anticancer, analgesic, sedative, and anti-inflammatory properties. These findings highlight the potential of green-synthesized IONPs as promising candidates for various biomedical applications. However, further research is needed to fully understand their mechanisms of action, assess long-term safety, and explore additional applications, paving the way for their translation into clinical practice and improving healthcare outcomes.

Acknowledgements: This work was primarily supported by the National Key R&D Program of China (2021YFE0100300). The authors also thank the Pakistan Science Foundation for funding this research under project number PSF/CRP/18th Protocol (02).

Funding information: The Pakistan Science Foundation funded this project under Project number PSF/CRP/18th Protocol (02).

Author contributions: Abdur Rauf (AR): conceptualization, analysis, supervision, Zubair Ahmad (ZA): experimental, writing original draft, Haiyuan Zhang (HZ): Conceptualization, supervision, Naveed Muhammad (NM): biological screening, analysis, Zuneera Akram (ZA): data curation, software, and Inamuddin (IM): software writing and editing. All authors read and approved this article for submission.

Conflict of interest: Authors state no conflict of interest.

Data availability statement: The datasets generated during and/or analyzed during the current study are available from the corresponding author on reasonable request.

References

[1] Ali A, Zafar H, Zia M, ul Haq I, Phull AR, Ali JS, et al. Synthesis, characterization, applications, and challenges of iron oxide nanoparticles. Nanotechnol Sci Appl. 2016;9:49–67.

[2] Amstad E, Textor M, Reimhult E. Stabilization and functionalization of iron oxide nanoparticles for biomedical applications. Nanoscale. 2011;3:2819–43.

[3] Rahman MM, Khan SB, Jamal A, Faisal M, Aisiri AM. Iron oxide nanoparticles. Nanomaterials. 2011;3:43–67.

[4] Gudkov SV, Burmistrov DE, Serov DA, Rebezov MB, Semenova AA, Lisitsyn AB. Do iron oxide nanoparticles have significant antibacterial properties? Antibiotics. 2021;10:884.

[5] Aljohny BO, Ahmad Z, Shah SA, Anwar Y, Khan SA. Cellulose acetate composite films fabricated with zero-valent iron nanoparticles and its use in the degradation of persistent organic pollutants. Appl Organomet Chem. 2020;34:e5892.

[6] Rukhsar M, Ahmad Z, Rauf A, Zeb H, Ur-Rehman M, Hemeg HA. An overview of iron oxide (Fe3O4) nanoparticles: From synthetic strategies, characterization to antibacterial and anticancer applications. Crystals. 2022;12:1809.

[7] Gour A, Jain NK. Advances in green synthesis of nanoparticles. Artif Cells Nanomed Biotechnol. 2019;47:844–51.

[8] Mukherjee A, Sarkar D, Sasmal S. A review of green synthesis of metal nanoparticles using algae. Front Microbiol. 2021;12:693899.

[9] Bahrulolum H, Nooraei S, Javanshir N, Tarrahimofrad H, Mirbagheri VS, Easton AJ, et al. Green synthesis of metal nanoparticles using microorganisms and their application in the agrifood sector. J Nanobiotechnol. 2021;19:1–26.

[10] Hussain I, Singh N, Singh A, Singh H, Singh S. Green synthesis of nanoparticles and its potential application. Biotechnol Lett. 2016;38:545–60.

[11] Saleem H, Zengin G, Locatelli M, Mollica A, Ahmad I, Mahomoodally FM, et al. *In vitro* biological propensities and chemical profiling of *E. milii* Des Moul (Euphorbiaceae): A novel source for bioactive agents. Ind Crop Prod. 2019;130:9–15.

[12] Yadav SC, Pande M, Jagannadham M. Highly stable glycosylated serine protease from the medicinal plant *E. milii*. Phytochemistry. 2006;67:1414–26.

[13] Chohan TA, Sarfraz M, Rehman K, Muhammad T, Ghori MU, Khan KM, et al. Phytochemical profiling, antioxidant and antiproliferation potential of *E. milii* var.: Experimental analysis and in-silico validation. Saudi J Biol Sci. 2020;27:3025–34.

[14] Ramli NR, Yusoff HM, Maulidiani M, Asari A, Wahab NHA. Stability of green synthesis of silver nanoparticles by using *E. milii* (Euphorbiaceae) leaves extract with different solvents and polarities. Malays J Anal Sci. 2023;27:766–76.

[15] Bouafia A, Laouini SE. Green synthesis of iron oxide nanoparticles by aqueous leaves extract of Mentha Pulegium L.: Effect of ferric chloride concentration on the type of product. Mater Lett. 2020;265:127364.

[16] Priya N, Kaur K, Sidhu AK. Green synthesis: An eco-friendly route for the synthesis of iron oxide nanoparticles. Front Nanotechnol. 2021;3:655062.

[17] Parveen K, Banse V, Ledwani L. Green synthesis of nanoparticles: Their advantages and disadvantages. In AIP Conference Proceedings. AIP Publishing; 2016.

[18] Shen T, Wang Q, Liu C, Yu F, Yu D, Li C. *E. milii* extract-mediated zinc oxide nanoparticles and their antinociceptive, muscle relaxant, and sedative activities for pain management in pediatric children. Appl Nanosci. 2020;10:1297–303.

[19] Bawazeer S. Green synthesis of silver nanoparticles from *E. milii* plant extract for enhanced antibacterial and enzyme inhibition effects. Int J Health Sci. 2024;18:25.

[20] Kanagasubbulakshmi S, Kadirvelu K. Green synthesis of iron oxide nanoparticles using Lagenaria siceraria and evaluation of its antimicrobial activity. Def Life Sci J. 2017;2:422–7.

[21] Rauf A, Khan A, Uddin N, Akram M, Arfan M, Uddin G, et al. Preliminary phytochemical screening, antimicrobial and antioxidant activities of *E. milii*. Pak J Pharm Sci. 2014;27:947.

[22] Sharma JN, Pattadar DK, Mainali BP, Zamborini FP. Size determination of metal nanoparticles based on electrochemically measured surface-area-to-volume ratios. Anal Chem. 2018;90:9308–14.

[23] Gul A, Fozia, Shaheen A, Ahmad I, Khattak B, Ahmad M, et al. Green synthesis, characterization, enzyme inhibition, antimicrobial potential, and cytotoxic activity of plant mediated silver nanoparticle using Ricinus communis leaf and root extracts. Biomolecules. 2021;11:206.

[24] Khan ST, Malik A, Wahab R, Abd-Elkader OH, Ahamed M, Ahmad J, et al. Synthesis and characterization of some abundant nanoparticles, their antimicrobial and enzyme inhibition activity. Acta Microbiol Immunol Hung. 2017;64:203–16.

[25] Shamim S, Gul S, Rauf A, Rashid U, Khan A, Amin R, et al. Gemifloxacin-transition metal complexes as therapeutic candidates: antimicrobial, antifungal, anti-enzymatic, and docking studies of newly synthesized complexes. Heliyon. 2022;8:e10378.

[26] Rauf A, Bawazeer S, Naseer M, Alhumaydhi FA, Aljohani AS, Habib A, et al. *In vitro* α-glycosidase and urease enzyme inhibition profile of some selected medicinal plants of Pakistan. Nat Prod Res. 2021;35:5434–9.

[27] Arshad A, Rehman T, Saleem H, Khan S, Saleem M, Tousif MI, et al. *In vitro* enzyme inhibition, antibacterial, UHPLC-MS chemical profiling and in silico studies of Indigofera argentea Burm. f. for potential biopharmaceutical application. South Afr J Bot. 2021;143:322–9.
[28] Rauf A, Khan R, Khan H, Jehan N, Akram M, Ahmad Z, et al. *In vitro* antimalarial and xanthine oxidase inhibition of 2-Aminoanthraquinone. Pak J Pharm Sci. 2016;29:429–32.
[29] Rahman H, Rauf A, Khan SA, Ahmad Z, Alshammari A, Alharbi M, et al. Green synthesis of silver nanoparticles using Rhazya stricta Decne extracts and their anti-microbial and anti-oxidant activities. Crystals. 2023;13:398.
[30] Chavez-Esquivel G, Cervantes-Cuevas H, Ybieta-Olvera L, Briones MC, Acosta D, Cabello J. Antimicrobial activity of graphite oxide doped with silver against Bacillus subtilis, Candida albicans, Escherichia coli, and Staphylococcus aureus by agar well diffusion test: Synthesis and characterization. Mater Sci Eng: C. 2021;123:111934.
[31] Hussain M, Ishfaq S, Sultan S, Jan A, Ahmad Z. Antimicrobial and cytotoxic potential of Anemone tetrasepala Royle. Phytopharmacol Res J. 2023;2:41–8.
[32] Shahab Khan M, Ahmad M. *In vitro* antimicrobial activity of Rumex Dentatus L. (Polygonaceae) plant extracts. Phytopharmacol Res J. 2022;1:32–42.
[33] Khan R, Quradha MM, Saif AQ, Ali J, Rauf A, Khan A. Comparative urease enzyme inhibition profile of leaves and stems of Rumex nervosus vahl. Nat Prod Res. 2014;28:2355–7.
[34] Uddin G, Rauf A, Al-Othman AM, Collina S, Arfan M, Ali G, et al. Pistagremic acid, a glucosidase inhibitor from Pistacia integerrima. Fitoterapia. 2012;83:1648–52.
[35] Bawazeer S, Rauf A, Shah SUA, Ullah N, Uddin G, Khan H, et al. Antioxidant and Enzyme inhibitory activities of extracts and phytochemicals isolated from Pistacia integerrima. J Med Spice Plants. 2019;23:55–8.
[36] Alam M, Uddin G, Rashid U, Rauf A, Raza M, Shah SMM, et al. *In vitro* and in silico xanthine oxidase inhibitory potential of Benzofuran isolated from Viburnum grandiflorum Wall. Ex DC. S Afr J Bot. 2021;143:359–62.
[37] Supino R. MTT assays. In: O'Hare S, Atterwill CK, editors. In vitro toxicity testing protocols. Methods in Molecular Biology™, vol 43. Humana Press; 1995. p. 137–49.
[38] Burhan A, Kamaruddin M, Ahmad R, Marzuki I. Anticancer and cytotoxic potentials of Vernonia amygdalina Delile on WiDr cell lines. Phytopharmacol Res J. 2022;1:1–7.
[39] Muhammad N, Saeed M, Khan H. Antipyretic, analgesic and anti-inflammatory activity of Viola betonicifolia whole plant. BMC Complement Altern Med. 2012;12:1–8.
[40] Rauf A, Al-Awthan YS, Khan IA, Muhammad N, Ali Shah SU, Bahattab O, et al. In vivo anti-inflammatory, analgesic, muscle relaxant, and sedative activities of extracts from Syzygium cumini (L.) skeels in mice. Evid Based Complement Altern Med. 2022;2022:6307529.
[41] Bawazeer S, Rauf A. In vivo anti-inflammatory, analgesic, and sedative studies of the extract and naphthoquinone isolated from Diospyros kaki (persimmon). ACS Omega. 2021;6:9852–6.
[42] Bhatia P. Comparison study of iron and iron-oxide nanoparticles for thermoplasmonic applications. Mater Today Commun. 2023;35:106008.
[43] Hussain A, Yasar M, Ahmad G, Ijaz M, Aziz A, Nawaz MG, et al. Synthesis, characterization, and applications of iron oxide nanoparticles. Int J Health Sci. 2023;17:3.
[44] Persson K. Materials data on zno2 (sg:205) by materials project, 7. 2014. An optional note.
[45] Glazyrin K. Iron in oxides, silicates and alloys under extreme pressure-temperature conditions. Dissertation. Universität Bayreuth, Fakultät für Biologie, Chemie und Geowissenschaften, Bayreuth, Germany; 2011.
[46] Saqib S, Munis MFH, Zaman W, Ullah F, Shah SN, Ayaz A, et al. Synthesis, characterization and use of iron oxide nano particles for antibacterial activity. Microsc Res Tech. 2019;82:415–20.
[47] Jounaki K, Soltani KM, Vahidi H, Barabadi H. Bioengineering of nanomaterials using biological resources: biofabrication mechanisms, characterizations, and biomedical applications. In Bioengineered nanomaterials for wound healing and infection control. Cambridge, UK: Elsevier; 2023. p. 239–86.
[48] Khan S, Rauf A, Aljohani AS, Al-Awthan YS, Ahmad Z, Bahattab OS, et al. Green synthesis of silver and gold nanoparticles in Callistemon viminalis extracts and their antimicrobial activities. Bioprocess Biosyst Eng. 2024;47:1–15.
[49] Nayak D, Chopra H, Chakrabartty I, Saravanan M, Barabadi H, Mohanta YK. Opportunities and challenges for bioengineered metallic nanoparticles as future nanomedicine. In: Barabadi H, Saravanan M, Mostafavi E, Vahidi H, editors. Bioengineered nanomaterials for wound healing and infection control, Woodhead publishing series in biomaterials. Cambridge, UK: Woodhead Publishing; 2023. p. 517–40. doi: 10.1016/B978-0-323-95376-4.00012-5.
[50] Zare EN, Zheng X, Makvandi P, Gheybi H, Sartorius R, Yiu CK, et al. Nonspherical metal-based nanoarchitectures: synthesis and impact of size, shape, and composition on their biological activity. Small. 2021;17:2007073.
[51] Tahir A, Saeed A, Ramzan I, Hayat SS, Ahmad W, Naeem S, et al. Mechanism for the formation of magnetite iron oxide nanostructures by Ficus carica dried fruit extract using green synthesis method. Appl Nanosci. 2021;11:1857–65.
[52] Chan YB, Aminuzzaman M, Rahman MK, Win YF, Sultana S, Cheah S-Y, et al. Green synthesis of ZnO nanoparticles using the mangosteen (Garcinia mangostana L.) leaf extract: Comparative preliminary *in vitro* antibacterial study. Green Process Synth. 2024;13:20230251.
[53] Selvanathan V, Aminuzzaman M, Tan LX, Win YF, Cheah ESG, Heng MH, et al. Synthesis, characterization, and preliminary *in vitro* antibacterial evaluation of ZnO nanoparticles derived from soursop (Annona muricata L.) leaf extract as a green reducing agent. J Mater Res Technol. 2022;20:2931–41.
[54] Katata-Seru L, Moremedi T, Aremu OS, Bahadur I. Green synthesis of iron nanoparticles using Moringa oleifera extracts and their applications: Removal of nitrate from water and antibacterial activity against Escherichia coli. J Mol Liq. 2018;256:296–304.
[55] Sivakami M, Renuka R, Thilagavathi T. Green synthesis of magnetic nanoparticles via Cinnamomum verum bark extract for biological application. J Environ Chem Eng. 2020;8:104420.
[56] Yusefi M, Shameli K, Ali RR, Pang SW, Teow SY. Evaluating anticancer activity of plant-mediated synthesized iron oxide nanoparticles using Punica granatum fruit peel extract. J Mol Struct. 2020;1204:127539.